PCCP

PAPER

View Article Online
View Journal | View Issue

Cite this: *Phys. Chem. Chem. Phys.*, 2022, **24**, 29413

Phase behaviour of model triglyceride ternary blends: triolein, tripalmitin and tristearin†

Luca Pellegrino,[a] Gunjan Tyagi,[a] Eric S. J. Robles [b] and João T. Cabral *[a]

We investigate the phase behavior of model ternary triacylglycerol blends, comprising triolein ($C_{57}H_{104}O_6$, OOO), tripalmitin ($C_{51}H_{98}O_6$, PPP) and tristearin ($C_{57}H_{110}O_6$, SSS), building upon extensive characterisation of single and binary mixtures, in order to rigorously map the thermal transitions of model natural 'fats'. A combination of calorimetry, X-ray diffraction, and FTIR spectroscopy is employed to determine crystallisation and melting temperatures and identify the corresponding phases in the complex ternary system. We recover the eutectic behaviour of SSS-PPP blends and the invariability of OOO neat transitions, and resolve the complex β′ + β ternary surface, reflecting the roles of unsaturation and polymorphism of its constituents. Our results provide a representation of the OOO:PPP:SSS:temperature phase behaviour into a triangular prism, consistent with binary pair-wise data, which can inform a range of food science, cosmetic, pharmaceutical and cleaning applications that depend strongly on the physical-chemistry of such multicomponent 'triglycerides'.

Received 26th May 2022,
Accepted 16th November 2022

DOI: 10.1039/d2cp02395d

rsc.li/pccp

1 Introduction

Natural fat is a complex mixture of triacylglycerols, TAGs (commonly known as 'triglycerides'), free fatty acids (FAs) and phospholipids, and, if unrefined, minor quantities of sterols and tocopherols.[1] TAGs are formed by one glycerol unit esterified by fatty acids in all three OH positions. The physical properties of refined natural fats are largely dominated by the properties of the constituent TAGs, with various possible permutations of the three fatty acid chains. A precise determination of a single melting point of 'fat' is thus not trivial, and a melting range is often observed, characterised by waxy and pasty consistencies arising from a distribution of diverse mixed crystals.[2] The broad TAG distribution and associated crystallisation regimes also define their specific rheological properties[3] between solid and liquid states, modulated by the liquid fraction, composed of low molecular weight and/or unsaturated TAGs,[4,5] that is interstitial or encapsulated within the solid phases, even at sub-zero Celsius temperatures.[6–8] Homotriacylglycerols, constituted by three identical FA chains, such as tristearin (SSS),[9–11] tripalmitin (PPP)[12–15] and triolein (OOO),[16,17] have been extensively investigated with a range of experimental techniques, mainly powder X-ray diffraction (XRD), differential scanning calorimetry (DSC), dilatometry and infrared (IR) and Raman spectroscopies.[18–20] These are generally taken as model constituents of complex fats, comprising a range of hetero TAGs with numerous positional and structural isomers, to rationalise fat crystallisation behaviour and associated polymorphism. TAGs are often classified into three basic polymorphic forms, namely α, β′ and β,[21] each characterised by a specific carbon chain packing and thermal stability.[22] Most fats and triglycerides possess an α form, though often very unstable; others possess only a stable β′ form and no β form, and *vice versa*.[23] When present, transformations take place from α to β′ to β, upon heating; the existence of various phases is predicated, however, on the thermal history upon cooling. Although single TAGs provide a nice physical model, natural fats are constituted by mixtures of different TAGs, determining their complex phase behaviour. Detailed studies of TAG blends are of special interest for the science and engineering of food,[24] cosmetics, pharmaceuticals, *etc.*, as main constituents of end-products, or as matrices in which other chemical species are dispersed.[25] There are extensive literature studies examining the phase behaviour of binary mixtures of TAGs,[1,26–28] and in particular of saturated TAGs such as SSS and PPP, their mixing behaviour[14,29,30] and identification of accompanying crystal phases. Furthermore, the interaction of saturated and unsaturated TAGs, namely SSS–OOO or PPP–OOO, has been investigated to elucidate their miscibility.[31–34] In general, binary solid mixtures of components that are miscible in the liquid state can yield a homogeneous solid solution phase, a eutectic system, or result in compound formation, depending on two key factors, namely polymorphism and chain–chain interactions.

[a] *Department of Chemical Engineering, Imperial College London, London, UK. E-mail: j.cabral@imperial.ac.uk*
[b] *Procter & Gamble, Newcastle Innovation Centre, Newcastle upon Tyne, UK*

† Electronic supplementary information (ESI) available. See DOI: https://doi.org/10.1039/d2cp02395d

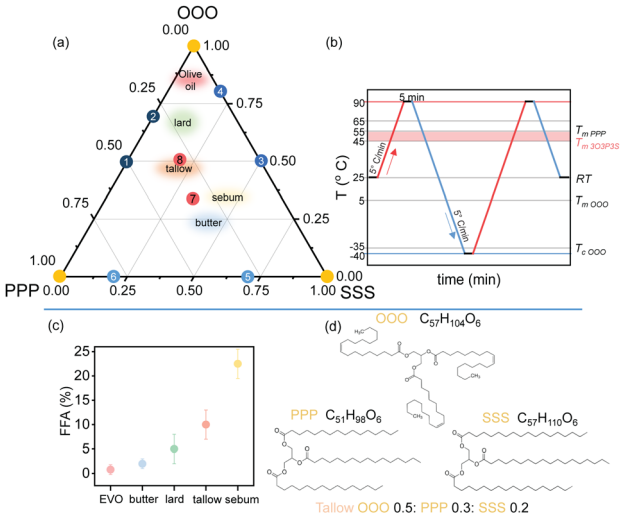

Fig. 1 (a) Ternary phase space for the investigated triglyceride blends (full circles), literature data (hollow circles) indicating the mass fractions of triolein (OOO), tripalmitin (PPP), and tristearin (SSS); pure components are shown in yellow, binary blends (1–6) in blue, and ternary blends in red. Typical compositions of naturally occurring fats are indicated alongside the ternary blends. Blend 8 is formulated as a synthetic analogue of natural 'beef tallow' (0.5 : 0.3 : 0.2 OOO : PPP : SSS). (b) Thermal profile employed in the blend characterisation, showing the relevant crystallisation and melting temperatures of pure components; (c) free fatty acid content[35] of selected blends shown above; and (d) molecular structure of the OOO, PPP and SSS triglycerides.

Despite their importance, considerably less is known about ternary TAG blends, and no complete phase diagrams have been reported. A classical study of the OOO:PPP:SSS system from 1912[36,37] provides reasonable estimates of the melting point, but does not consider the polymorphic nature of TAGs, which was not known at the time (in fact, X-ray crystallography was reported by von Laue a few weeks prior to its publication in the same year). In this study, we describe the ternary phase behaviour of a model OOO–PPP–SSS ternary blends. We take into account the polymorphism of the single TAGs and their binary blends, combining experimental and previous literature data as the foundation to provide a detailed description of the ternary phase behaviour, focusing on the effect of the unsaturated component OOO on the PPP–SSS saturated system by means of DSC, XRD and FTIR. The investigated ternary phase space is reported in Fig. 1(a), including the pure TAGs (yellow circles), the binary blends (blue circles) and the experimental ternary blend explored in this study (red circles). To benchmark our results with the previous literature data we repeat the characterisation of pure TAGs and selected OOO–SSS, OOO–PPP and PPP–SSS binary blends, numbered in the phase diagram. In the phase diagram are also indicated the approximate compositions of a range of natural fats described in terms of their OOO–PPP–SSS content with increasing unsaturation fraction towards pure OOO. Evidently, polymorphism, intersolubilty and phase behavior of a blend will be affected by different isomeric permutations of TAGs[26,37–40] and, for the current system, 27 possible permutations are conceivable. Therefore, in this simplified, yet comprehensive description, we take OOO, PPP, and SSS as coarse-grained representations of the homotriglycerides and all respective O, P and S isomeric permutations with a majority O, P or S fatty acid chains. Due to the sensitivity to thermal processing, which impacts the crystallisation and melting processes, and to ensure reproducibility and comparability of experimental data, all TAGs and blends were characterised following the same thermal program depicted in Fig. 1(b). To further understand the complexity of natural fats, the respective FFA content is reported in Fig. 1(c) and the molecular structures of the OOO, PPP and SSS triglycerides employed in this work are shown in Fig. 1(d). Our findings, incorporate the prior literature on single triglycerides and their binary blends, and provide a rigorous description of the ternary blend phase behaviour into a triangular prism, including the effect of polymorphism on melting and crystallisation behaviours.

2 Experimental

2.1 Triacylglycerols (TAGs)

Glyceryl trioleate, ≥99% (CAS 122-32-7), glyceryl tripalmitate ≥99% (CAS 555-44-2), and glyceryl tristearate ≥99% (CAS 555-43-1) were supplied by Merck KGaA and employed with no further purification. Prior to experimental characterisation, pure TAGs were heated at 90 °C to erase any thermal history, recrystalised at 5 °C min^{-1} and stored 4 °C.

2.2 Binary and ternary blend preparation

TAGs binary and ternary blends were prepared by combining the pure triglycerides in the prescribed ratio in a glass vial, mixed thoroughly using a vortex stirrer and then heated at 90 °C to ensure complete melting of all the components. The melting temperature was chosen prior to differential scanning calorimetry (DSC) and optical microscopy analysis (OM). Once molten, the blend is mixed once more using a magnetic stirrer and finally cooled and stored at 4 °C.

2.3 Characterisation

Differential scanning calorimetry (DSC) was performed employing a PerkinElmer DSC 8000 power compensation calorimeter using 40 μL aluminium pans. The TAGs as neat or blended were subjected to the temperature program reported in Fig. 1(b). Specifically, the samples were equilibrated at 25 °C for 5 min, a first heating cycle up to 90 °C at 5 °C min^{-1} to ensure complete melting, a 5 min hold at 90 °C, a first cooling to −40 °C at 5 °C min^{-1}, a 5 min hold at −40 °C and a second heating to 90 °C. Fourier transform infrared spectroscopy (FTIR) was carried out in attenuated total reflection mode (ATR), by means of a Bruker INVENIO-S equipped with a Platinum ATR on solid TAG samples. 64 spectra were acquired per sample from 4500 to 450 cm^{-1} at a resolution of 4 cm^{-1}, at room temperature after cooling the TAG samples from 90 °C at 5 °C min^{-1}. Variable temperature FTIR analysis on ternary TAG blends was performed by heating the samples from 25 °C to 90 °C at 5 °C min^{-1}.

X-Ray diffraction (XRD) was performed by means of a PANalytical X'Pert Pro powder diffractometer (theta/theta) equipped with a Cu anode long fine focus ceramic tube, (Kα = 1.54 Å, tension of 40 kV, current 20 mA). TAG samples were analysed at room temperature following the same temperature profile reported for the FTIR analysis, finely pulverised and back-loaded in a zero-diffraction plate. This method helps reducing the preferred orientation if the sample particles are not spherical, and it produces a relatively smooth surface, with a controlled thickness of about 2.5 mm. The XRD data were acquired by scanning a $4^\circ \leq 2\theta \leq 90^\circ$ range at 2° intervals, and 1 min aquisition per data point.

3 Results and discussion

3.1 Characterisation of neat TAGs

The characterisation of neat triglycerides OOO, PPP and SSS is reported in Fig. 2, and DSC melting profiles (Fig. 2(a)) show the transitions between the relevant crystal polymorphs. These results, included here for reference, are in good agreement with extensive previous literature on neat TAGs.[10,14,15,17] The α phase is obtained by fast-cooling from the melt (*viz.* 5 °C min^{-1} or higher) to temperatures well below the melting point of the α phase (below ≈−30 °C for OOO and ≈45 °C for PPP and SSS). Upon heating OOO from low temperature, the α phase melts, enabling the crystallization of a β′ phase, which in turn melts, enabling the crystallization of a β phase around −8 °C, which melts at ≈5 °C. The polymorphism of OOO has been previously investigated in detail.[41,42] It does not appear possible to obtain the β′ phase by continuously heating from the α phase of PPP and SSS, as a consequence of the very fast α to β transition. The β-phase can be obtained from either the α-phase, from the intermediate β′-phases, or from the melt; with the α-to-β being the fastest transition. Upon heating, the α-phase starts to melt, followed by a rapid crystallisation of the β phase. In the case of SSS, the crystallisation is characterized by two distinct exothermic processes, both related to the formation of the β-phase. Upon further heating the process remains exothermic until the melting of the β polymorph starts.

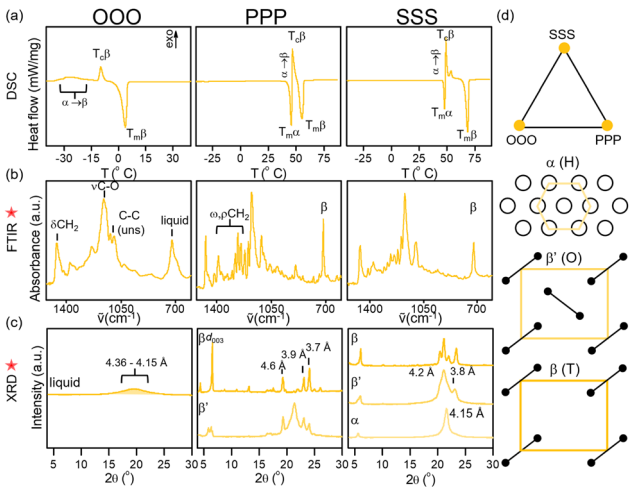

Fig. 2 Characterisation of neat TAGs. (a) DSC thermograms reporting the second heating of OOO, PPP and SSS at 5 °C min^{-1}, of the thermal profile in Fig. 1(b). (b) FTIR spectra of the 'fingerprint' region (1500–650 cm^{-1}) following the temperature profile, indicated in Fig. 1(b). (c) XRD profiles, measured at room temperature, showing the three principal polymorphs α, β′ and β. The top XRD patterns in each panel were obtained following the thermal profile (*), cooling at 5 °C min^{-1}, resulting in a β phase for PPP and SSS; OOO is in the liquid phase at this temperature. The second XRD profile (cooling at 25 °C min^{-1}), shown for PPP and SSS, resulted in β′; while the third XRD profile (cooling at 50 °C min^{-1}), shown only for SSS, yields the α phase. (d) Ternary composition diagram showing the three neat components and schematics of the α (H, hexagonal), β (T, triclinic) and β′ (O, orthorombic) polymorphs.

Fig. 2(b) depicts the fundamental vibrational modes of neat TAGs in the 'fingerprint' region at 25 °C (full-range FTIR analysis in the ESI,† Fig. S1). The FTIR spectrum of OOO exhibits broad infrared absorption bands in comparison to PPP and SSS, which exhibit sharp, intense peaks in the region. Mainly the frequency of the CH_2 bending or ''scissoring'' band is dependent upon the methylene chain packing and conformation. Disordered liquid-like chains exhibit a considerably broadened and relatively lower intensity scissoring band in the region of 1468–1466 cm^{-1}, while its shift and sharpening suggest ordering of the methylene chains approaching that of a crystalline geometry. Further changes in the CH_2 'rocking' mode of the triglyceride chains, which depends upon the inter chain interactions are indicative of structural alterations. For OOO, the absorption peak appears at 720 cm^{-1}, indicating a hexagonal unit cell, whereas a sharper absorption peak appears at 717 cm^{-1}, characteristic of a triclinic parallel unit cell. The saturated PPP and SSS on the other hand, display a larger number of sharp peaks *i.e.* from 1400 to 1100 cm^{-1} (C–H in plane bending, wagging ω and rocking ρ mode) whose number is equal to half of the number of CH_2 of the fatty acid chains.[43] The three basic polymorphs α, β′ and β, have distinct wide angle X-ray diffraction patterns as displayed in Fig. 2(c) and the schematic of the three crystal cages in Fig. 2(d). In general, a TAG α phase is characterized by a single strong reflection at 4.15 Å [$(2\theta) = 21.4^\circ$] of the hexagonal packing.[17] The β′ phases are characterized by an orthorhombic packing, which results in two strong reflections around 4.2 and 3.8 Å, [respectively $(2\theta) = 21.1^\circ$ and $(2\theta) = 23.3^\circ$]. The β-phase (triclinic) is identified by a very strong reflection at 4.6 Å, ($(2\theta) = 19.4^\circ$) and two other strong reflections at 3.9 and 3.7 Å ($(2\theta) = 23.1^\circ$ and $(2\theta) = 24.1^\circ$). The three reflections at 4.6, 3.9 and 3.7 Å correspond, respectively, to the (010), (110) and (100) planes of the subcell. The *d*-spacing is identified for PPP and SSS by a single d_{003} reflection at 15.3 Å ($(2\theta) = 5.78^\circ$).

3.2 Binary TAGs blends

The composition of the reference binary blends indicated in the phase diagram in Fig. 3(b) are given in Table 1. Blends 1 and 2 are OOO:PPP blends at two different ratios, 3 and 4 OOO:SSS blends and 5 and 6 PPP:SSS blends. The DSC thermograms are reported in Fig. 3(a) the OOO blends 1–4, show a single melting peak due to the β structure of either PPP or SSS. For blends 1 and 2, the OOO melting profile reduces to a single melting of

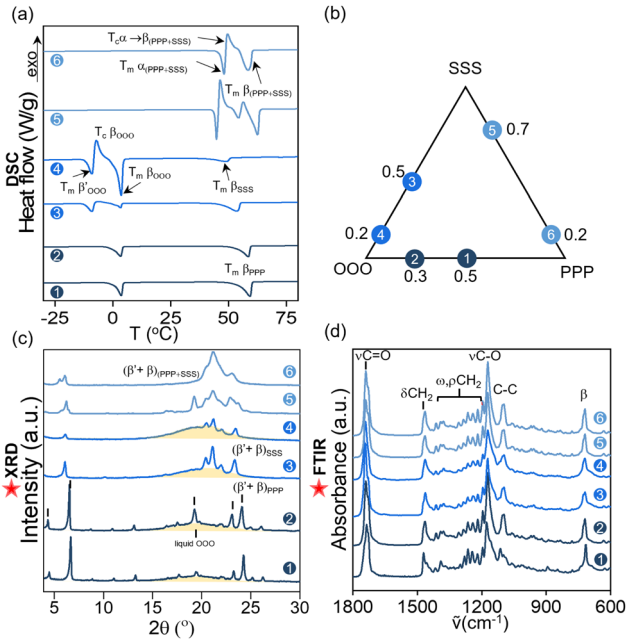

Fig. 3 Binary TAG blend characterisation. The binary blends compositions are described in Fig. 1(a) and in Table 1 and numbered from 1 to 6. (a) DSC thermograms of the second heating (5 °C min^{-1}) for different binary blends. (b) Triangular diagram describing the composition in OOO, PPP and SSS for different binary blends. (c) Room temperature XRD patterns of blend 1 to 6, showing the characteristic reflection for the different crystal structures identified. (d) Room temperature FTIR of the binary blends with assignments for the characteristic absorption bands.

Table 1 Binary and ternary blend compositions of OOO, PPP and SSS, prepared in mass fraction (w/w). For the isopleth, x = 0.001, 0.005, 0.01, 0.015, 0.020, 0.025, 0.03, 0.04, 0.05, 0.06, 0.07, 0.08, 0.1, 0.2, 0.3, 0.4, 0.5, 0.6, 0.7, 0.8, 0.99

Blend	OOO	PPP	SSS
1	0.5	0.5	—
2	0.7	0.3	—
3	0.5	—	0.5
4	0.8	—	0.2
5	—	0.3	0.7
6	—	0.8	0.2
7	0.3(3)	0.3(3)	0.3(3)
8	0.5	0.3	0.2
Isopleth 3PPP:2SSS	x	$(1-x)3/5$	$(1-x)2/5$

the β phase, whereas for blends 3 and 4 the melting of the OOO β′ and the β′ → β crystallisation are also present, indicating a poorer miscibility of the SSS in OOO compared to PPP in OOO (blends 1 and 2). As expected, the enthalphies of the transitions reflect the blend stoichiometry. Saturate TAG blends 5 (SSS rich) and 6 (PPP rich) show phase changing and temperatures in accordance with the respective pure equivalents, although at slightly lower temperatures due to the coexistence of two crystalline phases. Additional information regrading the energy involved in the phase-change upon melting can be obtained by tracking the melting enthalpy ΔH_m. Melting enthalpies obtained by the integration of the DSC melting peaks for pure TAGs and binary blends are reported in the ESI,† Fig. S2.

The room temperature XRD patterns after thermal processing (indicated by a star in Fig. 1(b)) are reported in Fig. 3(c). For the OOO blends with either PPP or SSS, the reflections associated with mixed β′ + β phases are identified, following the characterisation in Fig. 2(c), and distinct from the liquid OOO phase, appearing as a 'halo' centered at $(2\theta) \sim 20°$. The presence of OOO does not provide additional reflections at low angle, meaning that the crystalline structure of the saturated components remains largely unchanged, even as the characteristic melting temperatures change. In addition, OOO provides a medium for crystalline PPP or SSS, where (β′ + β) crystals are dispersed. For blend 5 and 6, (0.7 : 0.3 PPP : SSS) and (0.8 : 0.2 PPP : SSS) respectively, the presence of two reflections at $2\theta \simeq 5.5°$ and 6.1° (d_{003}) indicates that PPP and SSS crystallise in a β′ + β phase rich in β′. From the RT FTIR spectrum in Fig. 3(d), the two-component system can be identified by the presence of a shoulder emerging in the C═O stretching area and, in OOO blends, the absorption bands in the 717–719 cm^{-1} (rocking CH_2, β′ + β triclinic and orthorombic) region are broadened and shifted to higher wavenumber (720–723 cm^{-1}).[43] Binary blends melting temperatures are plotted in the phase diagrams reported in Fig. 4, respectively for the OOO–PPP (a), PPP–SSS (b) and SSS–OOO systems (c). The experimental blends investigated in this work, extracted from DSC thermograms reported in Fig. 3(a), are labelled as blue full circles and triangles and are combined with DSC and dilatometry measurements form previous literature data[1,26,30,33,34,44] (hollow circles and triangles). In OOO–PPP blends, the increase in OOO w/w reduces the onset temperature of the endothermic transitions of PPP, decreasing from the initial value of 65 °C to about 40 °C. In turn, PPP also affects the onset of the β′ phase of OOO increasing it from −10 °C to −3 °C. In agreement with Hale *et al.*,[34] a plateau region for both triglycerides can be observed between 0.2 and 0.7 w/w OOO. Higher OOO content further reduces the onset the β PPP fusion temperature, and concurrently slightly increases the β′ OOO temperature. The β form of OOO, on the other hand, is largely unaffected by the presence of PPP at all concentrations, likely due to the greater stability and thermal reversibility of this polymorph. The presence of distinct melting points for the two triglycerides is indicative of phase separation, with possible partial miscibility at extreme concentrations, OOO-rich or PPP-rich, where a small upturn in β'_{OOO} has been reported.[14] Overall OOO–PPP is thus classified as a monotectic system (with partial solid solution at extremely high and low OOO fractions). By contrast, the PPP–SSS binary system is characterised by a eutectic temperature close to 64 ± 3°, with the minimum in the liquidus curve occurring at a composition between 16 and 25%, depending on the different techniques and resolution employed in previous reports.[26,33,45] Another feature of this system is the presence of non-eutectic, therefore continuous solid solution of the α and β′ phases, first reported by Lutton *et al.*[33] based on XRD and dilatometry measurements. The tendency for the lower melting point component to be dissolved to a greater extent, and for the

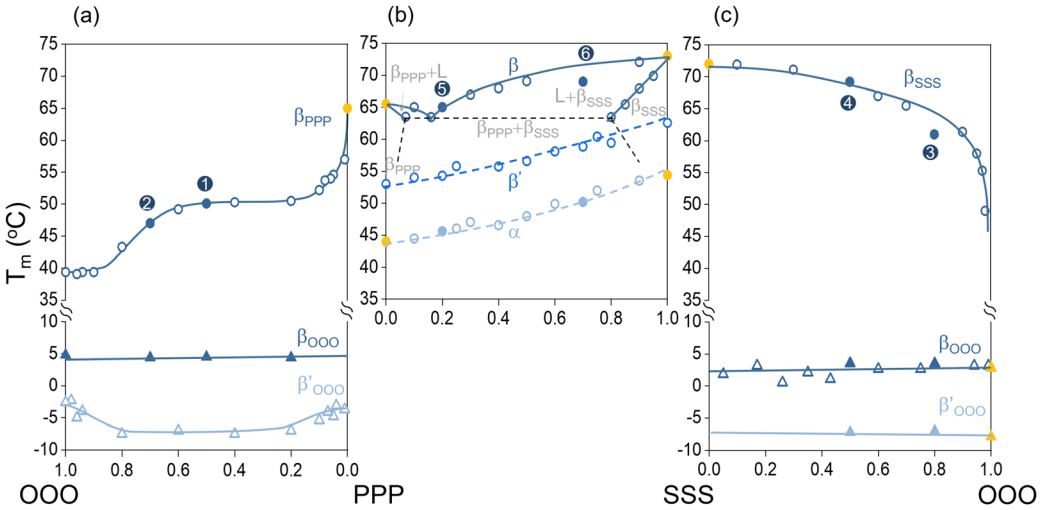

Fig. 4 Phase diagrams for the investigated binary blends (a) OOO–PPP, (b) PPP–SSS and (c) SSS–OOO. Melting temperatures 1–6 (full blue circles, triangles) T_m extracted from DSC measurements reported in Fig. 3(a). Experimental data in this work are combined with data from previous works (hollow blue circle, triangles) from ref. 30, 33, 34 and 44. Yellow symbols, triangles refer to the pure components. For OOO–PPP and SSS–OOO all the reported α and β phases are measurable upon cooling below 45 °C and reheating at 5 °C min^{-1}. The β′ phase reported in the (b) diagram can be formed cooling/annealing at 55 °C. In panels (a and c) there is no evidence of appreciable β and β′ transition temperatures in OOO induced by PPP and SSS.

eutectic point to be displaced towards a composition richest in the lower-melting component is commonly occurring in triglyceride mixtures. For the SSS–OOO system a similar behaviour to that of OOO–PPP system is observed, although the OOO melting point of both β′ and β forms is not lowered by the presence of SSS, denoting vanishing low solubility of SSS in solid OOO. The OOO is therefore included in the crystal lattice of SSS in weaker proportions (less than 2% w/w in the β phase) and the melting behaviour is similar to that of pure SSS.[44]

3.3 Ternary TAGs blends

The phase behaviour of ternary OOO–PPP–SSS mixtures is reported in Fig. 5 and the relative compositions in Table 1. The ternary phase diagram in Fig. 5(a) shows the ternary blends compositions investigated in this work, including an isopleth at a fixed ratio PPP/SSS = 1.5, progressively increasing the OOO weight fraction from 0.001 to 0.99 w/w, to evaluate the effect of the unsaturated triglyceride. This PPP/SSS ratio was selected due to its proximity to the eutectic (and has been originally identified as the eutectic[36]) of the binary system. Fig. 5(b) reports the XRD structural analysis carried on blends 7 (0.3 : 0.3 : 0.3 w/w OOO : PPP : SSS) and 8 (0.5 : 0.3 : 0.2 w/w OOO : PPP : SSS). The overall XRD reflections are given by the superposition of the liquid OOO phase and the $(\beta' + \beta)_{PPP+SSS}$ phase, as indicated for blend 7. In the high angle region, the bulging of the baseline given by the OOO liquid phase is more prominent in blend 8 due to the higher fraction of OOO with respect to the other components. The low angle region shows a single reflection for the d_{003} at 16.1 Å ($(2\theta) = 6.4^\circ$) indicating a possible β′ + β cocrystal of PPP and SSS. On the other hand, in blend 7 in the same regions the reflecion is split in two peaks at 15.8 and 16.2 Å, indicative of two defined crystal phases.

DSC characterisation of the explored ternary blends is shown in Fig. 5(c)–(e). Specifically, we focus on the high-melting region of the ternary bends Fig. 5(c), given by the phase transitions of the PPP–SSS pair because OOO transitions were not affected, as reported in Fig. 5(e) and already discussed for the binary blends. Fig. 5(d) reports the extracted melting temperature T_m for each phase identified in Fig. 5(c). Upon heating, at low OOO weight fractions (0.001–0.005 w/w) the phase behaviour is similar to that observed for binary blend 6 (PPP rich) with a common $\alpha_{(PPP+SSS)}$ phase quickly re-crystallising in a mixture of β and β′ forms expressed as (β′ + β), melting in two different phases, a lower melting at 60 °C ascribed to the PPP fraction $((\beta' + \beta)_{PPP})$ and a higher melting at 65 °C ascribed to the SSS fraction $((\beta' + \beta)_{SSS})$. Overall, the T_m profile of the (β′ + β) phase appears lower than the values recorded for the pure components, as already discussed for binary blends. In this case, however, the decrease is observed at much lower OOO fractions. As the OOO fraction increases (0.005 to 0.01), the metastable $\alpha_{(PPP+SSS)}$ melting peak is disappearing, re-crystallising and contributing to the (β′ + β) phase. This is observed in the DSC as a growing exothermic peak between the α and (β′ + β), until eventually disappearing at 0.06 w/w OOO. The T_m of PPP and SSS phases are initially reduced, then approaching a plateau region up to 0.1 w/w OOO. Here, until the full conversion of the α phase, is it possible to still identify the two (β′ + β) melting peaks for PPP and SSS, although progressively approaching and eventually merging into a single broad endothermic peak for 0.3 w/w OOO. At this stage, a single phase transition $((\beta' + \beta)_{(PPP+SSS)})$ is observed. This is interpreted to a solid solution of PPP and SSS crystals in an OOO liquid medium that destabilises and favours the rearrangement of the acyl chains into a more favourable packing. A further increase in the OOO weight fraction leads to the

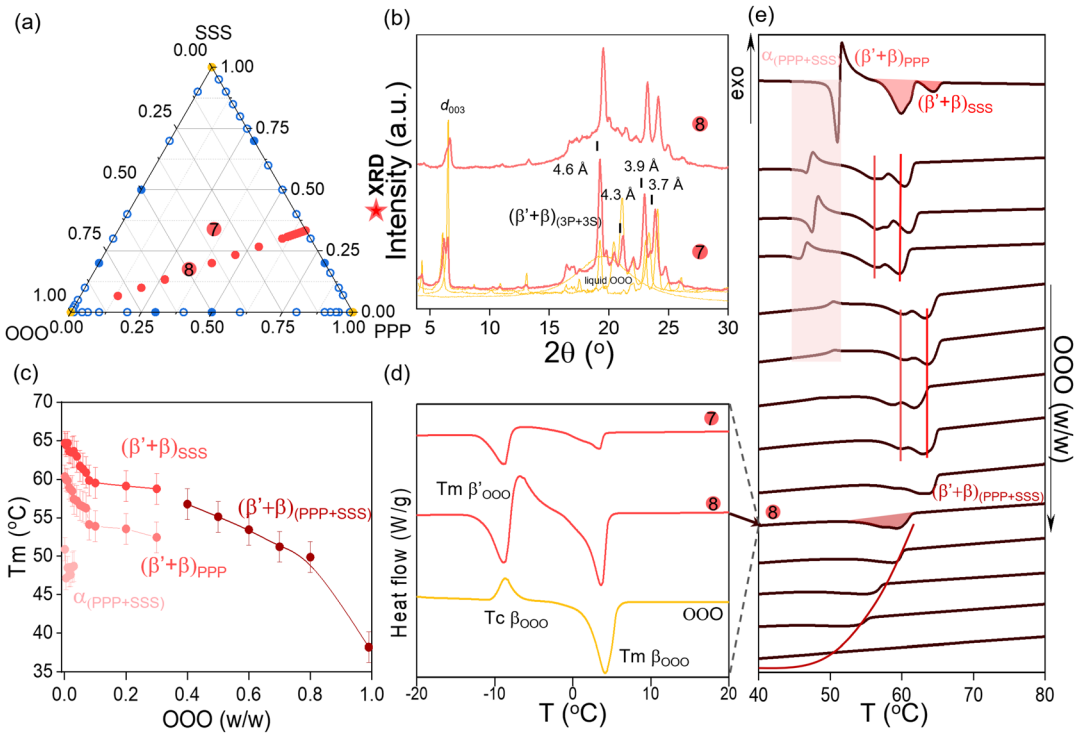

Fig. 5 Ternary blend characterisation. (a) Ternary phase diagram, reporting the composition of the investigated OOO:PPP:SSS blends (red full circles) alongside the compositional data for binary blends reported in Fig. 4 as full blue circle (experimental) and hollow blue circle (literature). The pure components are reported as full yellow circles. (b) Room temperature XRD patterns of blend 7 (0.3 : 0.3 : 0.3 w/w OOO : PPP : SSS) and 8 (0.5 : 0.3 : 0.2 w/w OOO : PPP : SSS), as case study for structural characterisation of ternary blends, with identified characteristic reflections for the different polymorphs. (c) DSC second heating thermograms for the ternary blends as function of OOO weight fraction (from 0.001 to 0.99); (d) melting temperatures T_m for the difference crystal phases extracted from the DSC thermograms in (c). (e) Detail of the low melting component of the blend OOO compared for blend 7, 8 and pure OOO.

same melting behaviour progressively moving towards lower T_m, until it is eventually no longer detectable for 0.99 w/w OOO. Due to the complex behaviour of the ternary mixture, assignment of the different phase transitions is not trivial, though we can summarise the addition of OOO to the PPP + SSS blend as follows:

- At low OOO w/w (0.001–0.005), the system behaves as a phase separated blend of PPP and SSS crystals incorporating small fractions of OOO;
- At intermediate OOO w/w (0.007 and 0.2), the PPP–SSS blend is not able to contain the liquid OOO, and the system rearranges towards a solid solution PPP + SSS with liquid OOO;
- For high OOO w/w (0.3–0.99), a single melting transition corresponding to the $(\beta' + \beta)_{(PPP+SSS)}$ solid solution is observed progressively at lower temperatures. The system behaves as a dispersion of PPP + SSS co-crystals in a continuous liquid OOO medium.

In the reference study of Kremann and Schoulz in 1912,[36] the melting behaviour of the OOO–PPP–SSS ternary system was described for the first time, including the diagram reproduced in the ESI,† Fig. S3, showing a maximum melting point of 64.4 °C corresponding to a mixture containing 0.303 : 0.07 : 0.627 OOO : PPP : SSS. These results, though extremely insightful, deviate from our results in Fig. 5(c), most likely due to the experimental method employed or the chemical purity of components; further, the polymorphic behaviour of TAGs was not considered, and instead a single, average melting temperature was recorded. In accordance with that observed for the PPP–SSS binary system, the authors report a binary eutectic in the ternary phase space at 0.42 w/w SSS (0.58 PPP) and melting at 54 °C. The ternary system is represented by contours defined by the melting points, with the eutectic forming a valley descending towards the pure OOO corner and vanishing at 0.9 w/w OOO. Although this representation could be a simpler guideline especially in understanding the liquidus phase boundary, the solidus lines and solid solutions formed cannot be inferred due to the lack of information and characterisation of the different polymorphs. Here, subsuming the knowledge gained from the binary phase diagram and the experimental results of ternary OOO:PPP:SSS blends, we report a comprehensive description of the phase behaviour of the ternary blends in the triangular prism, composition *vs.* temperature, shown in Fig. 6.

The boundaries of the phase space are defined by the β phases of the high-melting components compiled from the three binary blends reported in Fig. 4, OOO–PPP, PPP–SSS and SSS–OOO (blue spheres and lines). The ternary phase space (red) is built from the melting temperature data from Fig. 5(c), where the outer region is defined by the $(\beta' + \beta)_{SSS}$ and $(\beta' + \beta)_{(PPP+SSS)}$ transitions. The inner region is defined by the

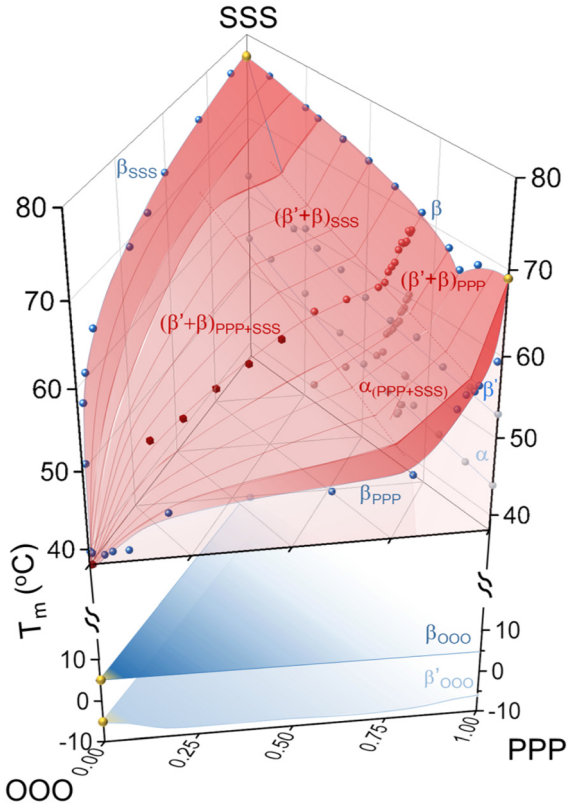

Fig. 6 3D ternary phase diagram built combining the experimental and literature data for pure components, binary and ternary blends reported respectively in Fig. 2, 4 and 5. The pure components are identified by yellow spheres, the binary and ternary blends by blue and red spheres respectively. The upper phase space identified the higher melting β form of the ternary blends (red areas) $(\beta' + \beta)_{SSS}$, $(\beta' + \beta)_{PPP+SSS}$ and for the binary blends (blue lines). The surface beneath shows the ternary phase transitions for $(\beta' + \beta)_{PPP}$ and $\alpha_{(PPP+SSS)}$ alongside binary PPP–SSS phase transitions β′ and α. The lower phase space reports the phase behaviour and thermal transition for the alpha and β forms of OOO.

$(\beta' + \beta)_{PPP}$ and $\alpha_{(PPP+SSS)}$ phases. The two phase region for low OOO weight fractions defines a depression followed by a plateau region in the $\beta' + \beta$ space, eventually leading to the PPP + SSS co-phase at high OOO loading. This behaviour defines a 'peritectic' region, usually observed only in mixed saturated/unsaturated systems where at least one triglyceride has two unsaturated acids as SOS/SOO or POP/POO.[1] In our representation, the PPP–SSS eutectic follows the (accurate) description made by Lutton[33] and we project its evolution in the ternary space with two horizontal red lines. We are able to describe, albeit in a simplified way, the different polymorphs for PPP and SSS and locate a new phase boundary, where most likely the eutectic extinguishes, at 0.4 : 0.4 : 0.2 w/w OOO : PPP : SSS and the co-phase $(\beta' + \beta)_{(PPP+SSS)}$ arises with a monotonic decrease in melting temperature as a function of the increase of the OOO content. All melting temperatures are found to be lower compared to the binary mixtures and pure components, therefore a depression can be identified, although distinct to that described by Kremann and Schoulz. As discussed in the binary and ternary blend characterisation, the OOO phase does not directly interact with the PPP + SSS system due to the distance in T_m. Therefore, in the ternary phase diagram the phase behaviour of the OOO β′ and β phases is described by means of triangular cuts defined by the respective melting temperature.

Natural fats are complex mixtures of triglycerides, fatty acids, and other minor components. Moving across the OOO tieline described in the ternary phase diagram allows us to explore different mixtures which, in OOO:PPP:SSS content, is approximate to the physical behaviour of several natural fats. In order to spatially resolve the structure and chemical interactions of the ternary TAG ternary constituents, we next consider a practically relevant, synthetic 'beef tallow' analogue. Natural beef tallow at ambient temperature exists as a mixture of β′ and β phases. Upon cooling from the melt, a β′(sub-α) phase is formed which transforms first in α and then to a mixture of α and β. At 16 °C, the α + β mixture is observed to transform into the normally observed β′ + β mixture noted above. Finally at 43 °C, the β phase disappeared leaving the β′ phase to melt at 48 °C. Thus beef tallow is a system characterised by a β phase which is not the highest melting phase.[1,37,46] According to our ternary space representation beef tallow can be simplified as a mixture of OOO : PPP : SSS in a 0.5 : 0.3 : 0.2 mass fraction. Therefore we produced a synthetic analogue of natural tallow, here referred to as blend 8, whose XRD structural characterisation and DSC are shown in Fig. 5. Additionally, we explored the melting behaviour of TAGs and in particular blend 8 to the molecular level. For this we took advantage of a Variable-Temperature Fourier-Transform Infrared spectroscopy (VT-FTIR) and FTIR-imaging. In VT-FTIR, a temperature ramp is applied to the sample by means of a controlled temperature stage where the sample is loaded, in reflection mode, between the torque screw and the diamond. The results are reported in Fig. 7, corresponding to spectra collected in continuous mode, heating from 25 °C to 75 °C at 5 °C min^{-1}, probing the full range of PPP and SSS melting temperatures.

From Fig. 7(a), in the three spectral regions the temperature increase is visualised by a transition from sharp and well defied absorption peaks to broader bands, typical of a solid to liquid phase transition and associated reduction in the conformational order. Specifically in the 'fingerprint' region, the C–H in-plane bending mode structure (1350 to 1180 cm^{-1}) typical of the solid β phase is lost and the spectra display a shift to lower wavenumbers and absorption bands similar to the liquid state of neat OOO at RT. The crystalline band centered at 718 cm^{-1} (inset), indicative of the crystal cage shifts from 717 cm^{-1}, associated with the β′ + β phase, to a broad absorption band centered at 722 cm^{-1}, indicating a mixed phase constituted by an increased fraction of hexagonal phases (720 cm^{-1}) in the liquid fraction. For the C=O and C–H regions, a shift to higher wavenumbers is observed. To track the evolution of the melting process, representative absorption shifts for each region were plotted as function of temperature, reported in Fig. 7(b). Specifically, for the "fingerprint region" we took the symmetric stretching of the ester group, ν_sCOOR, formed by one of the glycerol OH functional group and a COOH group from a fatty

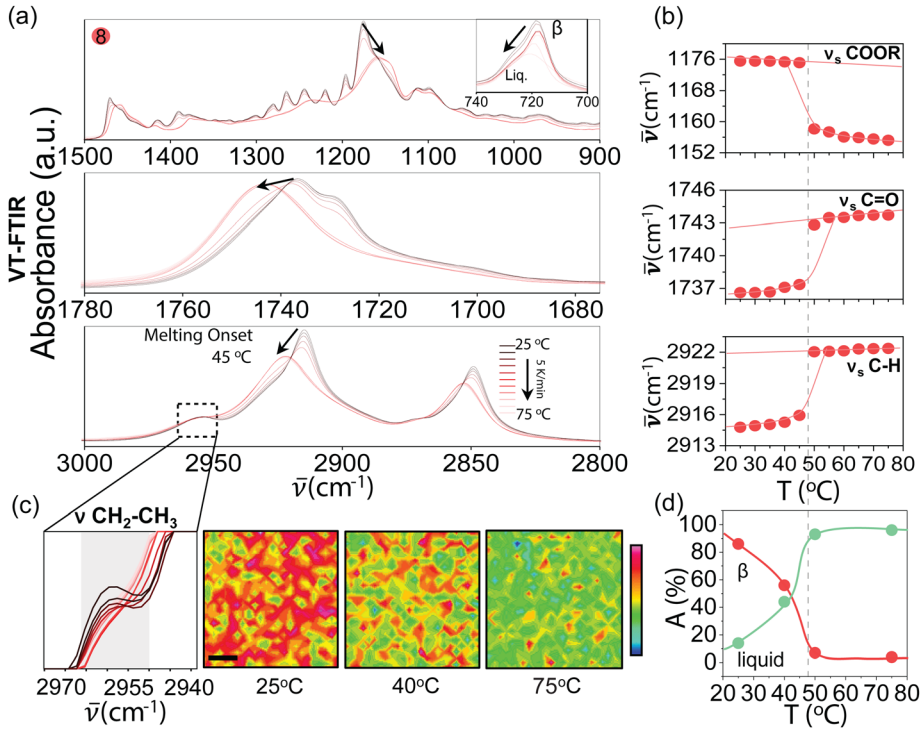

Fig. 7 Variable temperature FTIR characterisation of blend 8 (OOO : PPP : SSS 0.5 : 0.3 : 0.2) analogue in TAG components weight fraction to tallow. (a) VT-FTIR spectra of the 'fingerprint' region, C═O region and C–H region (top to bottom) recorded at 5 °C min^{-1} from 25 to 75 °C. (b) Wavenumber shifts for the stretching of the TAG ester ν_{COOR} (1150 cm^{-1} at room temperature, RT), stretching of C═O $\nu_{C=O}$ (1737 cm^{-1} at RT) and stretching of C–H ν_{C-H} (2915 cm^{-1} at RT) as a function of temperature. (c) FTIR imaging of the CH_2–CH_3 stretching associated with the CH_2 group adjacent to the terminal CH_3 in the fatty acid chains. 200 μm × 200 μm absorbance maps of the 2960 cm^{-1} at 25, 40 and 75 °C, with a resolution of 2 μm, report the evolution of the absorption band with temperature. (d) Areal coverage for the solid fraction (red) and liquid fraction (green) extracted from the IR imaging maps as a function of temperature.

acid chain; for the "C═O region", we considered the symmetric stretching ν_sC═O of the fatty acid carbonyl group; for the "C–H region" we took the symmetric stretching ν_sC–H of the fatty acids methylene groups. In all regions, a discontinuity is observed from 45 °C, indicating the onset of the melting process. From 50 to 55 °C and beyond, the shifts align to a new constant value. The red lines are guide to the eye, depicting a first-order solid to liquid phase transition. The simple nature of this transition implies the existence of no intermediate phases, since triglycerides cannot be brought into an amorphous solid state. The amorphous portion could be assigned to a bulk liquid state or it could be described in terms of a disordered portion of the crystallographic unit cell. To further explore the nature of the bulk liquid phase, we performed FTIR imaging of the CH_2-CH_3, reported in Fig. 7(c). This stretching band is associated with the CH_2 group adjacent to the terminal CH_3 in the fatty acid chains. Because TAGs pairing in the different crystal cages is determined by the alignment and orientation of the CH_2–CH_3 end groups, this absorption is ascribed to an ordered crystal phase and therefore not present in the liquid state. In Fig. 7(c), 200 μm × 200 μm absorbance maps of 2960 cm^{-1} at 25, 40 and 75 °C, with a resolution of 2 μm, report the evolution of the absorption band with temperature. The red area is associated with the high intensity peak that progressively disappears at high temperature, corresponding to the transition from an ordinate solid to an homogeneous bulk liquid (green) with crystal inclusions. These conclusions are quantified in Fig. 7(d), where a color deconvolution was performed on the FTIR maps extracting the red channel, associated with the solid portion and the green channel, associated with the liquid portion, with the areal coverage of each phase plotted as a function of temperature. The behaviour is again reminiscent of first order solid to liquid transition, although with a discontinuity not as sharp as that observed from the absorption shifts. This behaviour therefore represents not an order–disorder transition, but a gradual phase conversion with coexistence of both solid and liquid portions, even at temperature where the blend appears to be in a 'liquid' state. Further evidence of this melting behaviour is provided by polarised optical microscopy reported in Fig. S4 (ESI†), where changes in crystal morphology can be observed above the melting point of the blend, expected for the complex polymorphic behaviour of its components.

4 Conclusions

In this paper, we described the phase behaviour of ternary mixtures of triolein, tripalmitin and tristearin, which are key components of triacylglycerols found in naturally-occurring

'fats'. Despite the inherent complexity of natural systems, associated with their multicomponent nature, comprising various TAG isomers, as well as fatty acids and other lipids, it is possible to develop simpler synthetic analogues that capture their fundamental thermodynamic behaviour. Specifically, blends of OOO:PPP:SSS enable the description of a range of natural systems, by varying the relative TAG composition. We reported the experimental characterisation of pure TAGs and their binary mixtures with a range of techniques, namely DSC, XRD and FTIR, alongside previous literature data that corroborate and anchor our results. We provide a new characterisation and description of ternary mixtures, focusing on the effect of the unsaturated component on blend properties, and therefore reproducing the phase behaviour by means of simplified models mimicking natural fats such as butter, tallow, lard and oils. Combining the information gathered on pure TAGs and their binary and ternary mixtures from experiments and literature we built a comprehensive ternary phase diagram, describing the formation of the different crystal phases in the ternary OOO:PPP:SSS space as a function of the melting temperature. Taking a ''beef tallow'' analogue blend as a representative, illustrative blend, characterised by a 0.5 : 0.3 : 0.2 w/w in OOO : PPP : SSS we further investigate *via* variable temperature FTIR the nature of the crystal phases and their melting behaviour. We found, through FTIR imaging, that even at room temperature, portions of the blends appear in a liquid-like state (triolein) and how upon melting the blend undergoes a first order-like solid to liquid transition, where crystals are still present above the blend melting temperature. No evidence of the amorphous solid state is found but, instead, the system converts into a bulk liquid state, progressively disordering the crystalline cell of the high-melting components, resulting in crystal transformations into more stable polymorphs.

We expect our work to establish a multicomponent framework to describe the complex phase behaviour of TAG mixtures, in terms of the OOO–PPP–SSS ratio, enabling further studies, including the addition of fatty acids, or the role of specific isomers, which are intrinsic to naturally occurring TAGs. Moreover, the methodology can be exploited in the analysis of the melting behaviour of specific OOO:PPP:SSS combinations, as synthetic analogues of natural fats, such the one reported for ''beef tallow'', providing a route towards defining simpler descriptive models that are relevant to a range of food science, cosmetics, pharmaceutical and cleaning/removal applications, which depend strongly on the physical-chemical properties and thermal history of these blends.

Conflicts of interest

There are no conflicts to declare.

Acknowledgements

This work was supported by a research chair (JC) awarded by the Royal Academy of Engineering (UK), and by the Engineering and Physical Sciences Research Council [EPSRC, EP/V056891/1] and Procter & Gamble *via* the ANTENNA Prosperity Partnership.

References

1 R. Timms, *Prog. Lipid Res.*, 1984, **23**, 1–38.
2 H.-D. Belitz, W. Grosch and P. Schieberle, *Food Chem.*, 2009, 938–970.
3 S. S. Narine and A. G. Marangoni, *Food Res. Int.*, 1999, **32**, 227–248.
4 A. Wright, M. Scanlon, R. Hartel and A. Marangoni, *J. Food Sci.*, 2001, **66**, 1056–1071.
5 R. G. Jensen, A. M. Ferris and C. J. Lammi-Keefe, *J. Dairy Sci.*, 1991, **74**, 3228–3243.
6 J. Deman and A. Beers, *J. Texture Stud.*, 1987, **18**, 303–318.
7 D. Precht, *Crystallization and polymorphism of fats and fatty acids*, Marcel Dekker, New York, 1988, vol. 31.
8 R. Ball, *Phys. D*, 1989, **38**, 13–15.
9 E. Lutton, *J. Am. Chem. Soc.*, 1945, **67**, 524–527.
10 E. Da Silva, S. Bresson and D. Rousseau, *Chem. Phys. Lipids*, 2009, **157**, 113–119.
11 H. Mayama, *Soft Matter*, 2009, **5**, 856–859.
12 V. Hongisto, V.-P. Lehto and E. Laine, *Thermochim. Acta*, 1996, **276**, 229–242.
13 K. Sato and T. Kuroda, *J. Am. Oil Chem. Soc.*, 1987, **64**, 124–127.
14 M. Kellens, W. Meeussen and H. Reynaers, *J. Am. Oil Chem. Soc.*, 1992, **69**, 906–911.
15 M. Kellens, W. Meeussen and H. Reynaers, *Chem. Phys. Lipids*, 1990, **55**, 163–178.
16 C. Akita, T. Kawaguchi and F. Kaneko, *J. Phys. Chem. B*, 2006, **110**, 4346–4353.
17 R. Ferguson and E. Lutton, *J. Am. Chem. Soc.*, 1947, **69**, 1445–1448.
18 J. R. Dafler, *J. Am. Oil Chem. Soc.*, 1977, **54**, 249–254.
19 J. Hagemann, W. Tallent and K. Kolb, *J. Am. Oil Chem. Soc.*, 1972, **49**, 118–123.
20 J. Hagemann and J. Rothfus, *J. Am. Oil Chem. Soc.*, 1983, **60**, 1123–1131.
21 K. Larsson, *Acta Chem. Scand.*, 1966, **20**, 20.
22 L. Jensen and A. Mabis, *Acta Crystallogr.*, 1966, **21**, 770–781.
23 D. T. Hurle, *Handbook of crystal growth: Fundamentals. Thermodynamics and kinetics*, North-Holland, 1993.
24 K. Sato, *Chem. Eng. Sci.*, 2001, **56**, 2255–2265.
25 *Lipid Technologies and Applications*, ed. F. D. Gunstone and F. B. Fadley, Routledge, 2018.
26 J. Rossell, *Adv. Lipid Res.*, 1967, **5**, 353–408.
27 D. Chapman, *Chem. Rev.*, 1962, **62**, 433–456.
28 D. Small, *The Physical Chemistry of Lipids*, 1986, pp. 345–394.
29 C. Himawan, W. MacNaughtan, I. A. Farhat and A. G. Stapley, *Eur. J. Lipid Sci. Technol.*, 2007, **109**, 49–60.
30 W. MacNaughtan, I. Farhat, C. Himawan, V. Starov and A. Stapley, *J. Am. Oil Chem. Soc.*, 2006, **83**, 1–9.
31 W. Ng, *J. Am. Oil Chem. Soc.*, 1989, **66**, 1103–1106.
32 I. Norton, C. Lee-Tuffnell, S. Ablett and S. Bociek, *J. Am. Oil Chem. Soc.*, 1985, **62**, 1237–1244.
33 E. Lutton, *J. Am. Oil Chem. Soc.*, 1955, **32**, 49–53.
34 J. E. Hale and F. Schroeder, *Lipids*, 1981, **16**, 805–809.

35 S. Mahesar, S. Sherazi, A. R. Khaskheli and A. A. Kandhro, *et al.*, *Anal. Methods*, 2014, **6**, 4956–4963.
36 R. Kremann and R. Schoulz, *Monatsh. Chem. Verw. Teile Anderer Wiss.*, 1912, **33**, 1063–1076.
37 R. Timms, *Aust. J. Dairy Technol.*, 1980, **35**, 47.
38 V. Gibon, F. Durant and C. Deroanne, *J. Am. Oil Chem. Soc.*, 1986, **63**, 1047–1055.
39 M. Knoester, P. De Bruijne and M. Van Den Tempel, *Chem. Phys. Lipids*, 1972, **9**, 309–319.
40 L. Bouzidi and S. S. Narine, *Chem. Phys. Lipids*, 2012, **165**, 77–88.
41 L. Bayés-Garca, T. Calvet, M. À. Cuevas-Diarte, S. Ueno and K. Sato, *J. Phys. Chem. B*, 2013, **117**, 9170–9181.
42 G. J. Maximo, M. C. Costa, J. A. Coutinho and A. J. Meirelles, *RSC Adv.*, 2014, **4**, 31840–31850.
43 S. Parkash and J. Blanshard, *Spectrochim. Acta, Part A*, 1975, **31**, 951–957.
44 A. Desmedt, C. Culot, C. Deroanne, F. Durant and V. Gibon, *J. Am. Oil Chem. Soc.*, 1990, **67**, 653–660.
45 R. Kerridge, *J. Chem. Soc. (Resumed)*, 1952, 4577–4579.
46 U. Riiner, *Lebensm. Wiss. Technol.*, 1970, **3**, 101–106.